RSC Advances

PAPER

View Article Online
View Journal | View Issue

Cite this: *RSC Adv.*, 2023, **13**, 12386

Synthesis and photoluminescent characterization of ceramic phosphors $Li_2MgGeO_4:Ln^{3+}$ ($Ln^{3+} = Pr^{3+}$ or Tm^{3+}) under different excitation wavelengths

Nikola Bednarska-Adam,[a] Joanna Pisarska,[a] Marta Kuwik,[a] Tomasz Goryczka,[b] Maciej Zubko[b] and Wojciech A. Pisarski*[a]

Received 23rd January 2023
Accepted 14th April 2023

DOI: 10.1039/d3ra00500c

rsc.li/rsc-advances

In the current work, germanate phosphors $Li_2MgGeO_4:Ln^{3+}$ (Ln = Pr, Tm) have been synthesized and then investigated using luminescence spectroscopy. The X-ray diffraction analysis demonstrate that ceramic compounds Li_2MgGeO_4 containing Pr^{3+} and Tm^{3+} ions crystallize in a monoclinic crystal lattice. Luminescence properties of Pr^{3+} and Tm^{3+} ions have been examined under different excitation wavelengths. The most intense blue emission band related to the $^1D_2 \rightarrow {}^3F_4$ transition of Tm^{3+} is overlaps well with broad band located near 500 nm, which is assigned to F-type centers. These effects are not evident for Pr^{3+} ions. Ceramic phosphors $Li_2MgGeO_4:Ln^{3+}$ (Ln = Pr, Tm) are characterized based on measurements of the excitation/emission spectra and their decays. The experimental results indicate that germanate ceramics Li_2MgGeO_4 doped with trivalent rare earth ions can be applied as inorganic phosphors emitting orange (Pr^{3+}) or blue (Tm^{3+}) light.

Introduction

Germanate ceramics with olivine structure are promising inorganic compounds due to their excellent low-permittivity microwave dielectric properties, solid electrolytic properties for lithium-ion batteries and emission properties for modern visible or infrared photonics. In particular, germanate ceramics belonging to olivine-type family with general chemical formula Li_2MGeO_4, where M = Co,[1] Zn or Mg[2] are interesting from the scientific and technological points of view. They crystallized into an orthorhombic or monoclinic phase. Also, the reversible phase transformation monoclinic (low-temperature) ↔ orthorhombic (high-temperature) can occur. These ceramic systems are able to accommodate transition metals or rare earth ions and then can be applied as efficient phosphors emitting visible light or near-IR radiation. Recently published studies were limited to inorganic phosphors Li_2ZnGeO_4 (ref. 3 and 4) and Li_2MgGeO_4 (ref. 5 and 6) singly doped with Mn^{2+} emitting blue/green light. Moreover, olivine-type phosphors $(Li_x–Mg_{1-x})(Sc_x–Mg_{1-x})GeO_4$ singly doped with Cr^{3+} present tunable near-IR emission and have practical applications as light sources for nondestructive food analysis.[7] In contrast to transition metals, germanate ceramics with rare earth ions have not been often examined. Inorganic phosphors Li_2SrGeO_4 present enhanced emission through energy transfer process between Ce^{3+} and Tb^{3+}/Dy^{3+}.[8] The enhanced persistent blue emission was also realized in Li_2ZnGeO_4 phosphors by rare earth doping (Pr^{3+}, Nd^{3+}, Gd^{3+}).[9]

Among rare earths, the Pr^{3+} and Tm^{3+} ions are interesting optical dopants due to presence of several multicolor 4f–4f luminescent transitions. The increasing demand for crystalline and amorphous host matrices has promoted the researchers to develop various types of ceramic phosphors[10] and inorganic glasses[11] doped with Pr^{3+} and Tm^{3+} ions for their potential applications as luminescent materials. Trivalent Pr^{3+} ions can offer luminescence in the blue, green, red and white spectral ranges depending on the kind of host matrices. Luminescence properties of Pr^{3+} ions have been examined under ultraviolet[12] or blue light[13] irradiation. Most of the inorganic phosphors containing Pr^{3+} ions emit intense orange or red light.[14–16] Special attention has been paid to Pr^{3+} doped phosphors emitting white light.[17–19] Novel optical temperature sensor was also proposed based on emission of Pr^{3+} ions in $Ba_{0.7}Sr_{0.3}TiO_3$.[20] In contrast to Pr^{3+}, ceramic compounds doped with Tm^{3+} ions are known mainly as a blue-emitting phosphors.[21–24] Thulium doped inorganic phosphors could be also applicable in white light emitting diodes (wLEDs) through Dy^{3+} co-doping.[25]

Structural, thermal and optical properties of ceramics Li_2MgGeO_4 un-doped and doped with Er^{3+} and Ho^{3+} ions were described in our previous work.[26] Direct energy band gaps for Li_2MgGeO_4 with Er^{3+} and Ho^{3+} are found to be 5.67 and 5.77 eV and they are comparable to the values reported earlier.[5,6] Further results of the Rietveld refinement confirmed that Li_2MgGeO_4 crystallize in a monoclinic crystal lattice.[26] Here, we show preliminary results for ceramics Li_2MgGeO_4 doped with

[a]*Institute of Chemistry, University of Silesia, 9 Szkolna Street, 40-007 Katowice, Poland. E-mail: wojciech.pisarski@us.edu.pl*

[b]*Institute of Materials Engineering, University of Silesia, 75.Pułku Piechoty 1A Street, 41-500 Chorzów, Poland*

Pr^{3+} and Tm^{3+}. In particular, emission properties of rare earths have been analyzed under different excitation wavelengths. The experimental results suggest that germanate ceramics Li_2MgGeO_4 doped with rare earth ions can be applied as inorganic phosphors emitting orange (Pr^{3+}) or blue (Tm^{3+}) light.

Experimental

Synthesis

$Li_2Mg_{(100-x)}GeO_4$:xLn^{3+} (given in molar%), where Ln^{3+} denotes Pr^{3+} or Tm^{3+}, in the form of pellets have been synthesized *via* a conventional high-temperature solid-state reaction method. The concentration of Ln^{3+} was equal to 0.5 mol%. They are referred here as LMG-Pr and LMG-Tm, respectively. High purity initial reagents were Li_2CO_3 (99.997%), MgO (99.99%), GeO_2 (99.99%), and depending on the sample: Pr_2O_3 (99.999%) or Tm_2O_3 (99.999%). The stoichiometric amounts of raw materials in appropriate mass ratios were milled and homogenized thoroughly in an agate mortar for about 1 hour, with ethanol (POCH Basic 96% pure) as a medium. In the next step, grounded samples were calcinated in a non-covered platinum crucible at 1100 °C for 6 h in the air atmosphere to achieve decarbonization. Calcination was divided into two steps: reaching the temperature of 800 °C in 30 minutes, then getting to 1100 °C in 10 minutes. Subsequently, calcinated samples were grounded again and divided into smaller batches. Pellets (10 mm in diameter) were formed using PVA as a binder and cold pressed at 375 MPa. Prepared pellets were subjected to heat treatment to remove the binder at 550 °C for 2 hours (with a heating rate of 3 °C min^{-1}) under ambient air conditions. After cooling down to room temperature, the ceramic samples were sintered in the high-temperature furnace at 1200 °C for 5 h and naturally cooled down to room temperature in a closed furnace. The sintering process includes several steps: rise to 800 °C in one hour, then sintering for 15 minutes, heating up to 1200 °C (9 °C min^{-1}), and sintering for 3 hours.

Methods

In order to study germanate ceramics singly doped with praseodymium and thulium ions, several measurements at room temperature were performed, including XRD, SEM, excitation and photoluminescence spectra, and decay curves. Chromaticity coordinates were also calculated. The nature of the studied germanate ceramics was identified using an X'Pert-Pro diffractometer. All X-ray diffraction measurements were done with a use of the $CuK_{\alpha 1and2}$ radiation. The microstructure of samples was observed using JSM6480 scanning electron microscope (SEM) along with JSM-7100F TTL LV. Excitation and luminescence measurements were registered using laser equipment consisting of a Photon Technology International (PTI) Quanta-Master 40 (QM40) UV/VIS Steady State Spectrofluorometer coupled with a tunable pulsed optical parametric oscillator (OPO) pumped by the third harmonic of a Nd:YAG laser. The laser system included a double 200 mm monochromator, a xenon lamp as a light source, and a multimode UVVIS PMT R928 (PTI Model 914) detector. The spectra were registered with a resolution of ±0.5 nm. Decay curves with an accuracy of ±0.5 μs were recorded using the PTI ASOC-10 [USB-2500] oscilloscope (Horriba Instruments). It should be also pointed out that the Commission Internationale de I'Eclairage (CIE) chromaticity coordinates (x,y) and chromaticity diagram were calculated from the emission spectra and plotted using Color Calculator software.

Results and discussion

The X-ray diffraction patterns of the germanate ceramics Li_2MgGeO_4:Pr^{3+} (LMG-Pr) and Li_2MgGeO_4:Tm^{3+} (LMG-Tm) are presented in Fig. 1. The typical SEM micrographs of the studied ceramic samples are also shown.

The XRD analysis confirmed that all diffraction peaks can be well assigned to ceramic compounds crystallize in a monoclinic lattice with $P2_1/n$ space group, which is isostructural to Li_2ZnGeO_4 (ICDD PDF-4 database – card no 04-015-4929).[2] Moreover, no additional phases associated to impurities exist compared to pure Li_2MgGeO_4 monoclinic phase.[26] It evidently reveals that rare earth doping has no effect on the crystalline structure of germanate ceramics and Pr^{3+} (or Tm^{3+}) ions are well entered into the lattice Li_2MgGeO_4. The SEM images illustrate germanate samples LMG-Pr and LMG-Tm, which consist of micrometer-sized and irregular-shaped grains similar to ceramics Li_2MgGeO_4 containing Er^{3+} or Ho^{3+} ions.[26] Previous studies for $La_3Ga_5SiO_{14}$:Pr^{3+} phosphors well demonstrated that the crystalline grains in micron size and irregular morphology can be successfully observed and these effects are related to the high-temperature sintering process.[27] In our case, rare earth doping caused a reduction of the grain size compared to the un-

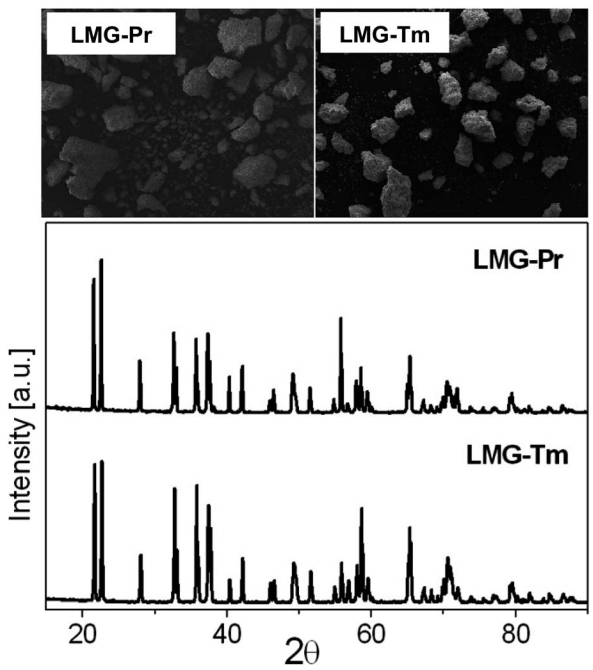

Fig. 1 The XRD patterns and SEM images of ceramic phosphors LMG-Pr and LMG-Tm.

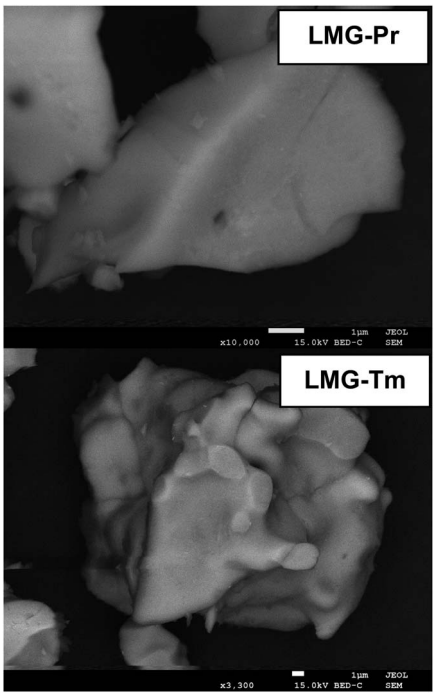

Fig. 2 Ceramic particles observed with SEM-BE images for ceramic phosphors LMG-Pr and LMG-Tm.

doped ceramics Li_2MgGeO_4 crystallized in a regular oval-like shape.[26] Moreover, the SEM-BS images for ceramic samples LMG-Pr and LMG-Tm are also presented in Fig. 2. It is an image sensitive to the contrast of the chemical composition. Objects presented in the images also have an even shade of gray. Such contrasts indicate that the components have reacted and only one crystalline phase is formed. There are no other precipitations, phases, or inclusions. The monophasic nature of the created germanate ceramics is confirmed by the X-ray diffraction patterns shown in Fig. 1. Considering all the above arguments, a conclusion can be drawn that designed ceramics have been received.

The photoluminescence spectra of the germanate ceramics Li_2MgGeO_4:Pr^{3+} (LMG-Pr) and Li_2MgGeO_4:Tm^{3+} (LMG-Tm) have been examined under different excitation wavelengths. The emission spectra are shown in Fig. 3.

The systematic studies indicate that luminescence spectra measured for LMG-Pr depend critically on the excitation wavelengths. The spectra excited between 370 and 433 nm range consist of broad low-intensity emission band centered at about 500 nm. The intensity of band decreases in direction to longer excitation wavelengths up to about 433 nm when broad emission of ceramic host is nearly quenched. When sample was excited above 435 nm, narrow luminescence lines characteristic for rare earth ions occur. The emission bands are related to transitions originating from the $^3P_0$ and $^1D_2$ excited states to the lower-lying states of trivalent praseodymium. The most intense emission transitions of Pr^{3+} are observed under excitation of 450 nm line and correspond to bands located in the blue and reddish-orange spectral ranges.

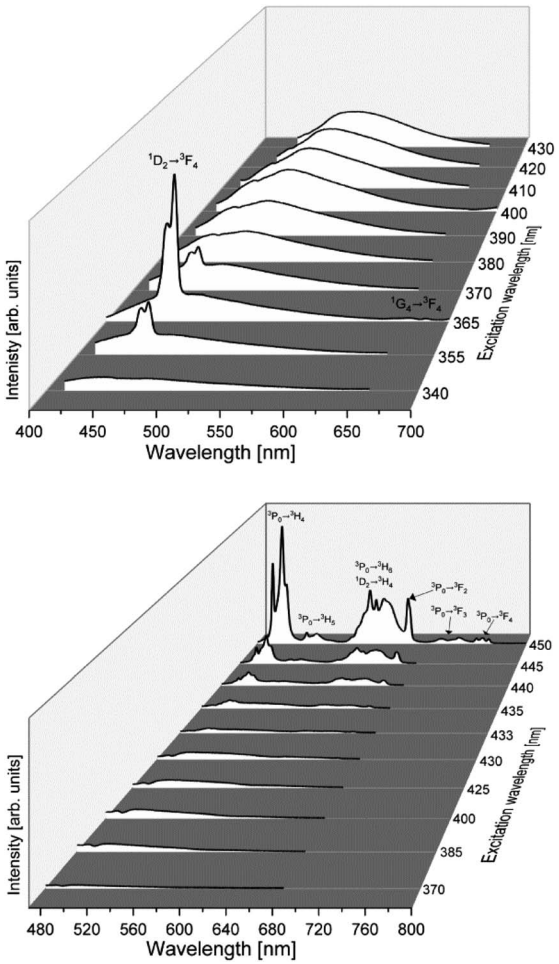

Fig. 3 The photoluminescence spectra of ceramic phosphors LMG-Pr (bottom) and LMG-Tm (top).

Completely different situation is observed for ceramics doped with Tm^{3+}. The photoluminescence spectra measured under excitation between 355 and 370 nm consist of narrow band corresponding to the $^1D_2 \rightarrow {}^3F_4$ blue transition of Tm^{3+} ions ($\lambda_p = 460$ nm), which is well overlapped with broad emission of ceramic host. The luminescence band of Tm^{3+} ions is the most intense, when the ceramic sample was excited at 365 nm. The band assigned to the $^1G_4 \rightarrow {}^3F_4$ transition of Tm^{3+} ions was also observed in the red spectral range, but its emission intensity is extremely low.

The obtained results were interpreted on the basis of the excitation and emission spectra measurements for ceramic samples un-doped and singly doped with Pr^{3+} and Tm^{3+} under selective excitation wavelengths. The excitation spectra were measured under monitoring emission wavelengths at 610 nm (LMG-Pr) and 460 nm (LMG-Tm). Fig. 4 shows the excitation and emission spectra measured for samples LMG, LMG-Pr and LMG-Tm, respectively.

Our previous spectroscopic investigations[26] revealed that luminescence spectrum measured for un-doped LMG consists of broad band located in the blue/green region with maximum peak emission near 500 nm depending on the excitation

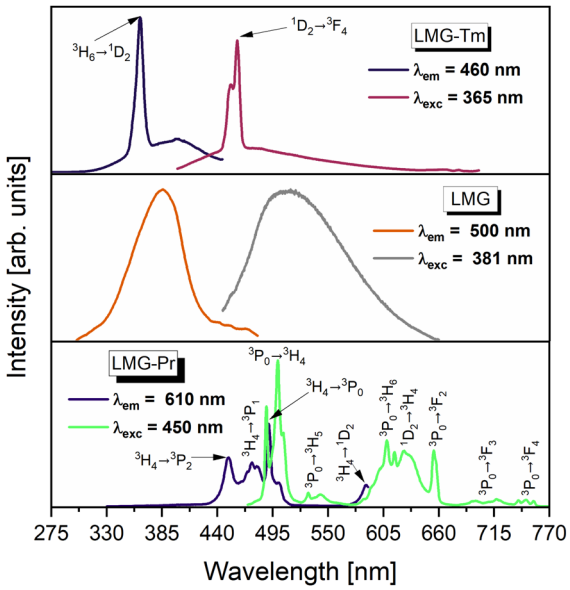

Fig. 4 The excitation and emission spectra of ceramic phosphors undoped (LMG) and doped with Pr^{3+} (LMG-Pr) and Tm^{3+} (LMG-Tm).

wavelength. Broad emission is associated to the occurrence of magnesium in LMG ceramic host. Similar effects were also observed earlier for MgO nanobelts[28] and MgO films[29] where blue/green emission was identified as defects and oxygen vacancies in magnesium oxide assigned to F-type centers. Thus, the excitation spectrum for un-doped LMG monitored under emission wavelength λ_{em} = 500 nm shows broad band near 380 nm (Fig. 4).

Characteristic emission bands of Pr^{3+} are well observed, when ceramic sample LMG-Pr was excited by 450 nm line. In this case, sample LMG-Pr was excited directly at $^3P_2$ state of Pr^{3+} and ceramic host LMG could be also pumped theoretically on the edge of its broad excitation band. However, characteristic broad band assigned to ceramic matrix is not evident in the emission spectrum of LMG-Pr under 450 nm excitation. Considering that fact we suggest that the ceramic host cannot be excited efficiently and the interaction between LMG matrix and Pr^{3+} ions is rather difficult to obtain contrary to sample LMG-Tm. When the excitation line 365 nm was used, ceramic sample LMG-Tm is excited simultaneously at $^1D_2$ state of Tm^{3+} ions and ceramic matrix. In this case, the excitation band $^1D_2$ (Tm^{3+}) is very close to the maximum of excitation band of ceramic host LMG. Thus, the luminescence band due to the $^1D_2 \rightarrow {}^3H_6$ (Tm^{3+}) transition is well overlapped with broad emission characteristic for ceramic host LMG. Therefore, we suggest that the excitation energy may be also transferred from ceramic host LMG to Tm^{3+}. The excitation spectra measurements confirms this hypothesis. The excitation spectrum measured under monitoring emission wavelength 460 nm ($^1D_2 \rightarrow {}^3H_6$ luminescent transition of Tm^{3+}) consists of two overlapped broad and narrow bands characteristic for ceramic host LMG and electronic transition originating from the $^3H_6$ ground state to the $^1D_2$ state of Tm^{3+}, respectively. These effects are not observed for LMG-Pr.

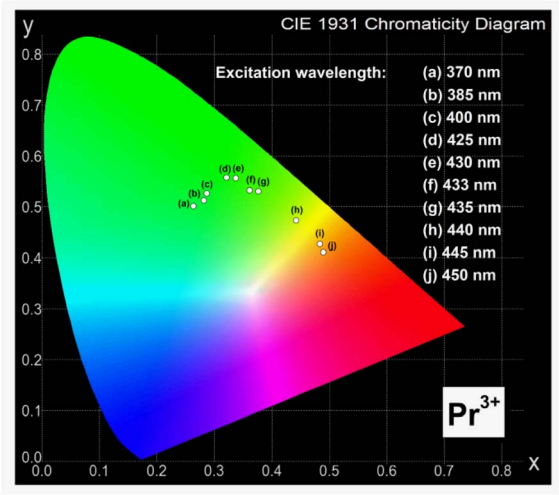

Fig. 5 The CIE chromaticity diagram of ceramic phosphors LMG-Pr.

In order to determine the color of emitting radiation for studied ceramic phosphors, the Commission Internationale de l'Eclairage (CIE 1931) chromaticity coordinates (x,y) were calculated from the emission spectra registered in the visible spectral range. The CIE diagrams for ceramic samples LMG-Pr and LMG-Tm varying with the excitation wavelengths are presented in Fig. 5 and 6.

According to previous studies, different ceramic phosphors containing praseodymium ions, such as $BaNb_2O_6$,[30] $CaWO_4$,[31] and Y_2MoO_6,[32] exhibit orange-red emission. However, results obtained for $Sr_{1.5}Ca_{0.5}SiO_4$,[33] $Ca_3Y_2Si_3O_{12}$,[34] and $CaSnO_3$ (ref. 35) show that chromaticity coordinates determined for system doped with Pr^{3+} ions correspond to green and greenish-blue region.

Our optical investigation indicates that the values of (x,y) for ceramic phosphors containing praseodymium ions strongly depend on the excitation wavelengths. They are changed from green to orange region with increasing excitation wavelength

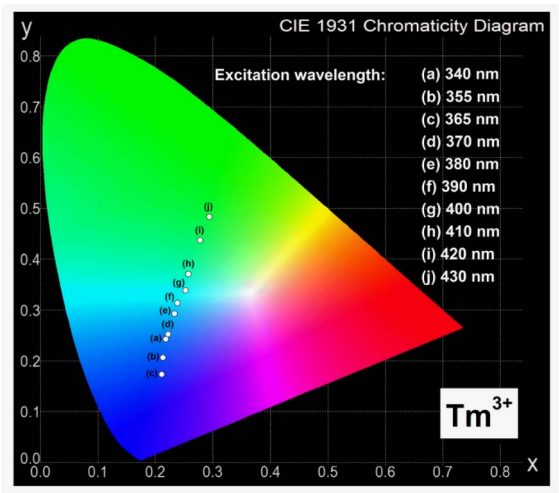

Fig. 6 The CIE chromaticity diagram of ceramic phosphors LMG-Tm.

from 370 nm to 450 nm. The intensities of emission lines due to characteristic transitions of Pr^{3+} are the highest for sample under 450 nm excitation. Thus, the chromaticity coordinates are due to the orange region of the CIE diagram. The evaluated chromaticity coordinates were similar to that of $YAl_3(BO_3)_4$.[36]

Similar situation is observed for ceramic phosphors doped with thulium ions, where the values of (x,y) also depend critically on the excitation wavelengths. They are changed from blue to green region, when the excitation wavelength increases from 340 nm to 430 nm. Previous studies for ceramic materials containing Tm^{3+} ions demonstrated well that phosphors like $LiLaSiO_4$ (ref. 37) and $BaMoO_4$ (ref. 38) can be used in blue light emitters. It was also confirmed by our optical results for ceramic phosphor Li_2MgGeO_4:Tm^{3+} excited at 365 nm, where the intensity of emission band due to the $^1D_2 \rightarrow {}^3H_6$ transition of thulium is the highest. Thus, the chromaticity coordinates calculated for Li_2MgGeO_4 doped with thulium ions correspond to the blue region of the CIE diagram. The results suggests that Li_2MgGeO_4 host can be successfully used as ceramic phosphors emitting orange (Pr^{3+}) or blue (Tm^{3+}) light under selective excitation wavelengths.

Luminescence decays from the excited states of rare earths in Li_2MgGeO_4 have been also studied. They are shown in Fig. 7.

For ceramic sample LMG-Pr luminescence decay curves were measured under excitation 450 nm and monitoring emission wavelength 610 nm. For sample LMG-Tm, the parameters were as follows: $\lambda_{exc} = 365$ nm, $\lambda_{em} = 460$ nm. Decay curves for samples LMG-Pr and LMG-Tm are well-fitted to a mono-exponential decay mode described by the equation $I(t) = I_0 \times \exp(-t/\tau)$, where $I(t)$ and I_0 are the luminescence intensities at time t and $t = 0$, respectively, while τ is the luminescence lifetime. Luminescence decay curve measured for ceramic host LMG under direct excitation 381 nm and monitoring emission wavelength 500 nm is also mono-exponential. Based on decay curve measurements, luminescence lifetimes for the ceramic host LMG and the excited states of rare earths were determined.

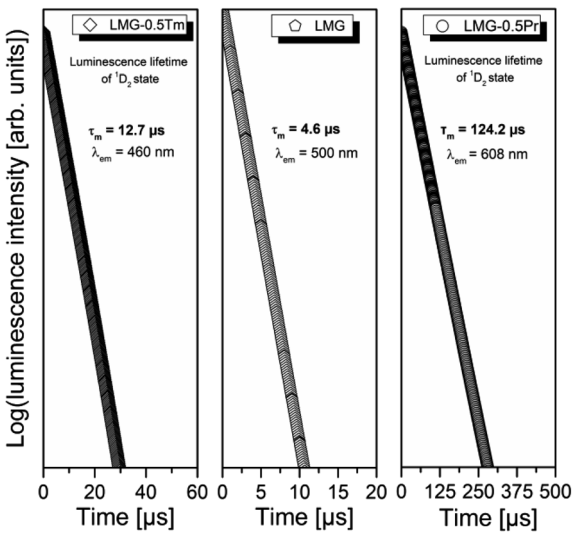

Fig. 7 The CIE chromaticity diagram of ceramic phosphors LMG-Tm.

For LMG and LMG-Tm ($^1D_2$ state of Tm^{3+}), the measured lifetimes are close to 4.6 μs and 12.7 μs, respectively. Similar to the $^1D_2$ (Tm^{3+}), the experimental values of emission lifetimes for the $^3P_0$ state of Pr^{3+} ions in numerous glasses and ceramics are very short and difficult to determine with relatively good accuracy. Here, the lifetime of Pr^{3+} is significantly longer and its value is equal to 124.2 μs. It suggests that luminescence is decayed from the lower-lying state $^1D_2$ (Pr^{3+}) in Li_2MgGeO_4.

Our previous studies for high-phonon borate glasses doped with Pr^{3+} ions[39] indicate that the excitation energy is transferred non-radiatively (multiphonon relaxation MPR) very fast from the $^3P_0$ state to the lower-lying $^1D_2$ state due to high-phonon energies and consequently reddish-orange luminescence corresponding to the $^1D_2 \rightarrow {}^3H_4$ transition of Pr^{3+} is observed, only. For lower-phonon germanate glasses doped with Pr^{3+} ions[40] two overlapped radiative transitions, *i.e.* short-lived $^3P_0 \rightarrow {}^3H_6$ and long-lived $^1D_2 \rightarrow {}^3H_4$ luminescent transitions of Pr^{3+} are existed in this spectral range. It could be attributed to the lower phonon energies and the increased radiative transition from the excited state $^3P_0$ (Pr^{3+}). This is a consequence of a substantial decrease in nonradiative multiphonon relaxation from the $^3P_0$ state to the lower-lying $^1D_2$ state of Pr^{3+}. Further luminescent experiments for LMG-Pr excited selectively at 450 nm ($^3P_0$ state) and 585 nm ($^1D_2$ state) confirm coexistence of both emission bands of Pr^{3+} ions in Li_2MgGeO_4 under blue pumping. Fig. 8 presents luminescence spectra of Pr^{3+} ions in ceramic host LMG in the orange-red range. The sample was pumped selectively by 450 nm and 585 nm excitation lines, respectively.

The spectrum measured for LMG-Pr under 585 nm excitation shows emission band related to the $^1D_2 \rightarrow {}^3H_4$ transition of Pr^{3+}. Completely different situation is observed for LMG-Pr excited at higher-lying state $^3P_0$ (Pr^{3+}) by 450 nm line, where several emission bands are present. Compared to the results obtained for sample excited at 585 nm, the emission spectrum

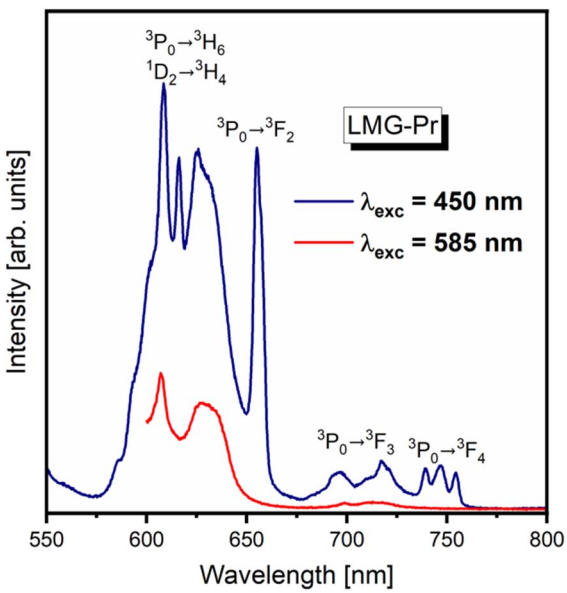

Fig. 8 Luminescence spectra of ceramic phosphors LMG-Pr excited at 450 nm ($^3P_0$ state) and 585 nm ($^1D_2$ state).

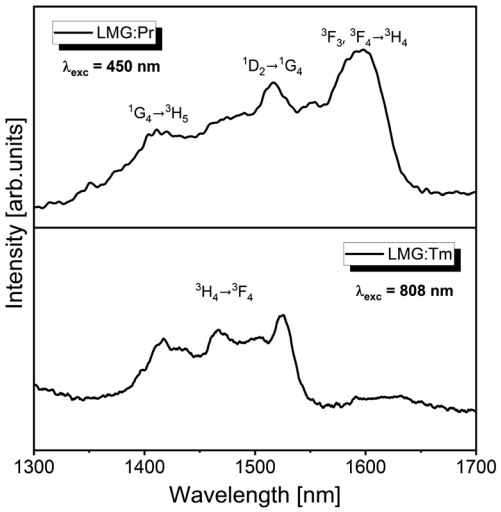

Fig. 9 Near-IR emission spectra of ceramic phosphors LMG-Pr and LMG-Tm.

consists of characteristic band due to the $^1D_2 \rightarrow {}^3H_4$ transition as well as additional bands corresponding to transitions from the $^3P_0$ state to the lower-lying states of Pr^{3+}. It proves that both $^3P_0$ and $^1D_2$ excited states of Pr^{3+} ions coexist in ceramic host Li_2MgGeO_4 under blue excitation.

Finally, germanate ceramics Li_2MgGeO_4:Ln^{3+} (Ln = Pr, Tm) have been examined for near infrared luminescence. From literature data it is well known that some ceramic materials synthesized in nano- or micrometric scale exhibit efficient luminescence in the second near-infrared window (NIR-II), which is important for numerous biomedical and optical applications.[41–48] Among rare earths, the Pr^{3+} (ref. 49) and Tm^{3+} (ref. 50) ions belong to promising optical dopants emitting radiation in the NIR-II region. However, inorganic phosphors with Pr^{3+} or Tm^{3+} have been rarely investigated for NIR-II luminescence. To the best of our knowledge, they are rather less documented in literature. Our optical studies indicate that both ceramic samples LMG-Pr and LMG-Tm show near-IR emission in the 1350–1650 nm spectral range.

Fig. 9 presents near-infrared luminescence spectra for samples LMG-Pr and LMG-Tm measured under excitation by 450 nm (Pr^{3+}) and 808 nm (Tm^{3+}) line, respectively. Luminescence spectrum for LMG-Tm consists of NIR band centered at about 1.47 μm, which corresponds to the $^3H_4 \rightarrow {}^3F_4$ transition of Tm^{3+}.[51] In contrast to LMG-Tm, three NIR luminescence bands are observed for sample LMG-Pr, which can be assigned to the $^1G_4 \rightarrow {}^3H_5$, $^1D_2 \rightarrow {}^1G_4$ and $^3F_3$, $^3F_4 \rightarrow {}^3H_4$ transitions of Pr^{3+}.[52] Our preliminary investigations demonstrate that Li_2MgGeO_4:Ln^{3+} (Ln = Pr, Tm) can be also applied as ceramic source emitting radiation in the NIR-II window. These phenomena will be the subject of further investigation.

Conclusion

Rare earth doped germanate ceramics Li_2MgGeO_4:Ln^{3+} (Ln = Pr, Tm) referred here as LMG-Pr and LMG-Tm have been prepared using solid-state reaction method and then studied using luminescence spectroscopy. The ceramic compounds Li_2MgGeO_4 doped with Pr^{3+} and Tm^{3+} ions crystallize in monoclinic crystal lattice, which was confirmed by X-ray diffraction analysis. Luminescence properties of trivalent rare earth ions have been analyzed under various excitation wavelengths. For sample LMG-Tm, the most intense blue emission band is due to the $^1D_2 \rightarrow {}^3F_4$ transition of Tm^{3+} and well overlapped with broad band centered at about 500 nm assigned to F-type centers. These effects are not evident for LMG-Pr. Based on measurements of the excitation/emission spectra and their decays, the experimental results for germanate ceramics Li_2MgGeO_4:Ln^{3+} (where Ln = Pr or Tm) are presented and discussed in details. It was suggested that germanate ceramics Li_2MgGeO_4 doped with trivalent rare earth ions can be applied as inorganic phosphors emitting orange (Pr^{3+}) or blue (Tm^{3+}) light. Further studies suggest that rare earth doped germanate phosphors Li_2MgGeO_4:Ln^{3+} (Ln = Pr, Tm) can be applied as ceramic sources emitting radiation in the second near-infrared window.

Conflicts of interest

There are no conflicts to declare.

Acknowledgements

The National Science Centre (Poland) supported this work under project No. 2019/35/B/ST5/01924.

References

1 S. B. Yahya, R. Barille and B. Louati, Synthesis, optical and ionic conductivity studies of a lithium cobalt germanate compound, *RSC Adv.*, 2022, **12**, 6602–6614, DOI: **10.1039/d2ra00721e**.

2 C. Li, H. Xiang, M. Xu, Y. Tang and L. Fang, Li_2AGeO_4 (A = Zn, Mg): Two novel low-permittivity microwave dielectric ceramics with olivine structure, *J. Eur. Ceram. Soc.*, 2018, **38**, 1524–1528, DOI: **10.1016/j.jeurceramsoc.2017.12.038**.

3 M. Shang, G. Li, D. Yang, X. Kang, C. Peng and J. Lin, Luminescence properties of Mn^{2+}-doped Li_2ZnGeO_4 as an efficient green phosphor for field-emission displays with high color purity, *Dalton Trans.*, 2012, **41**, 8861–8868, DOI: **10.1039/c2dt30670k**.

4 Y. Jin, Y. Hu, H. Duan, L. Chen and X. Wang, The long persistent luminescence properties of phosphors: Li_2ZnGeO_4 and Li_2ZnGeO_4:Mn^{2+}, *RSC Adv.*, 2014, **4**, 11360–11366, DOI: **10.1039/c3ra47760f**.

5 Y. Jin, Y. Hu, L. Chen, G. Ju, H. Wu, Z. Mu, M. He and F. Xue, Luminescent properties of a green long persistent phosphor Li_2MgGeO_4:Mn^{2+}, *Opt. Mater. Express*, 2016, **6**, 929–937, DOI: **10.1364/OME.6.000929**.

6 Y.-F. Zhu, T. Jiang, L. Li, L.-X. Cheng and J.-C. Zhang, Short-term non-decaying mechanoluminescence in Li_2MgGeO_4:Mn^{2+}, *Materials*, 2020, **13**, 1410, DOI: **10.3390/ma13061410**.

7 H. Cai, S. Liu, Z. Song and Q. Liu, Tuning luminescence from NIR-I to NIR-II in Cr^{3+}-doped olivine phosphors for nondestructive analysis, *J. Mater. Chem. C*, 2021, **9**, 5469–5477, DOI: 10.1039/d1tc00521a.

8 S. Huang and G. Li, Photoluminescence properties of Li_2SrGeO_4:RE^{3+} (RE = Ce/Tb/Dy) phosphors and enhanced luminescence through energy transfer between Ce^{3+} and Tb^{3+}/Dy^{3+}, *Opt. Mater.*, 2014, **36**, 1555–1560, DOI: 10.1016/j.optmat.2014.04.024.

9 T. Tu and G. Jiang, Enhanced persistent luminescence of Li_2ZnGeO_4 host by rare-earth ions (Pr^{3+}, Nd^{3+} and Gd^{3+}) doping, *J. Mater. Sci.: Mater. Electron.*, 2018, **29**, 3146–3152, DOI: 10.1007/s10854-017-8247-x.

10 S. Sailaja, S. J. Dhoble, C. N. Raju and B. S. Reddy, Emission analysis of Pr^{3+} and Tm^{3+}: $Ca_2Gd_2W_3O_{14}$ phosphors, *Physica B*, 2012, **407**, 103–107, DOI: 10.1016/j.physb.2011.09.133.

11 G. Dominiak-Dzik, W. Ryba-Romanowski, J. Pisarska and W. A. Pisarski, Spectral properties and dynamics of luminescent states of Pr^{3+} and Tm^{3+} in lead borate glasses modified by PbF_2, *J. Lumin.*, 2007, **122–123**, 62–65, DOI: 10.1016/j.jlumin.2006.01.098.

12 L.-G. Teoh, M.-T. Tsai, Y.-C. Chang and Y.-S. Chang, Photoluminescence properties of Pr^{3+} ion-doped $YInGe_2O_7$ phosphor under an ultraviolet irradiation, *Ceram. Int.*, 2018, **44**, 2656–2660, DOI: 10.1016/j.ceramint.2017.10.163.

13 H.-R. Shih, Y.-Y. Tsai, K.-T. Liu, Y.-Z. Liao and Y.-S. Chang, The luminescent properties of Pr^{3+} ion-doped BaY_2ZnO_5 phosphor under blue light irradiation, *Opt. Mater.*, 2013, **35**, 2654–2657, DOI: 10.1016/j.optmat.2013.08.007.

14 F. Chun, B. Zhang, H. Liu, W. Deng, W. Li, M. Xie, C. Luo and W. Yang, Na^+ and Pr^{3+} co-doped orange-emitting $CaYAl_3O_7$ phosphors: synthesis, luminescence properties and theoretical calculations, *Dalton Trans.*, 2018, **47**, 17515–17524, DOI: 10.1039/c8dt03828g.

15 S. Chawla, N. Kumar and H. Chander, Broad yellow orange emission from $SrAl_2O_4$:Pr^{3+} phosphor with blue excitation for application to white LEDs, *J. Lumin.*, 2009, **129**, 114–118, DOI: 10.1016/j.jlumin.2008.08.009.

16 T.-C. Liu, B.-M. Cheng, S.-F. Hu and R.-S. Liu, Highly stable red oxynitride β-SiAlON:Pr^{3+} phosphor for light-emitting diodes, *Chem. Mater.*, 2011, **23**, 3698–3705, DOI: 10.1021/cm201289s.

17 T.-C. Liu, B.-M. Cheng, S.-F. Hu and R.-S. Liu, Pr^{3+} doped $LaTiNbO_6$ as a single phosphor for white LEDs, *J. Alloys Compd.*, 2010, **492**, L61–L63, DOI: 10.1016/j.jallcom.2009.11.188.

18 T. Wei, W. Bo, C. Yan, C. Yeqing, L. Jun and Z. Qingguang, Single Pr^{3+}-activated high-color-stability fluoride white-light phosphor for white-light-emitting diodes, *Opt. Mater. Express*, 2019, **9**, 223–233, DOI: 10.1364/OME.9.000223.

19 T. Raghu Raman, Y. C. Ratnakaram and B. Deva Prasad Raju, Synthesis and spectroscopic investigations on Pr^{3+}-doped $LiPbB_5O_9$ phosphor for white LEDs, *Optik*, 2021, **225**, 165758, DOI: 10.1016/j.ijleo.2020.165758.

20 T. Wei, N. Haiyong, Z. Qiuhong and D. Jianhong, Novel optical temperature sensor based on emission in Pr^{3+} doped ferroelectric $Ba_{0.7}Sr_{0.3}TiO_3$, *RSC Adv.*, 2018, **8**, 23996–24001, DOI: 10.1039/c8ra04228d.

21 J. Liao, B. Qiu, H. Wen, J. Chen, W. You and L. Liu, Synthesis process and luminescence properties of Tm^{3+} in AWO_4 (A = Ca, Sr, Ba) blue phosphors, *J. Alloys Compd.*, 2009, **487**, 758–762, DOI: 10.1016/j.jallcom.2009.08.068.

22 L. Cai, L. Ying, J. Zheng, B. Fan, R. Chen and C. Chen, Luminescent properties of $Sr_2B_2O_5$: Tm^{3+}, Na^+ blue phosphor, *Ceram. Int.*, 2014, **40**, 6913–6918, DOI: 10.1016/j.ceramint.2013.12.012.

23 J. Li, H. Yan and F. Yan, A novel high color purity blue-emitting phosphor: $CaBi_2B_2O_7$:Tm^{3+}, *Mater. Sci. Eng., B*, 2016, **209**, 56–59, DOI: 10.1016/j.mseb.2016.03.004.

24 H.-R. Shih and Y.-S. Chang, A blue-emitting phosphor of Tm^{3+} ion-doped BaY_2ZnO_5, *J. Electron. Mater.*, 2017, **46**, 6603–6608, DOI: 10.1007/s11664-017-5717-0.

25 C. Wei, D. Xu, Z. Yang, Y. Jia, X. Li and J. Sun, Luminescence and energy transfer of Tm^{3+} and Dy^{3+} co-doped $Na_3ScSi_2O_7$ phosphors, *RSC Adv.*, 2019, **9**, 27817–27824, DOI: 10.1039/c9ra04727a.

26 N. Bednarska-Adam, J. Pisarska, M. Kuwik, E. Pietrasik, T. Goryczka, B. Macalik and W. A. Pisarski, Thermal, structural and optical properties of un-doped and lanthanide-doped germanate ceramics, *J. Alloys Compd.*, 2023, **934**, 167956, DOI: 10.1016/j.jallcom.2022.167956.

27 N.-N. Zhang, X.-X. Jiang, Y.-N. Wang, X.-R. Pan, Y.-Y. Zhang, B. Liu, Y.-G. Yang and X.-P. Wang, Synthesis, structure and luminescence characteristics of $La_3Ga_5SiO_{14}$:Pr^{3+} phosphors, *J. Alloys Compd.*, 2023, **932**, 167626, DOI: 10.1016/j.jallcom.2022.167626.

28 J. Zhang and L. Zhang, Intensive green light emission from MgO nanobelts, *Chem. Phys. Lett.*, 2002, **363**, 293–297, DOI: 10.1016/S0009-2614(02)01229-0.

29 C. Martínez-Boubeta, A. Martínez, S. Hernández, P. Pellegrino, A. Antony, J. Bertomeu, Ll. Balcells, Z. Konstantinović and B. Martínez, Blue luminescence at room temperature in defective MgO films, *Solid State Commun.*, 2011, **151**, 751–753, DOI: 10.1016/j.ssc.2011.03.007.

30 S. Jana, A. Mondal, J. Manam and S. Das, Pr^{3+} doped $BaNb_2O_6$ reddish orange emitting phosphor for solid state lighting and optical thermometry applications, *J. Alloys Compd.*, 2020, **821**, 153342, DOI: 10.1016/j.jallcom.2019.153342.

31 R. Paikaray, T. Badapanda, H. Mohapatra, T. Richhariya, S. N. Tripathy and N. Brahme, Investigation of structural, photoluminescence, and thermoluminescence properties of Praseodymium doped CaWO4 phosphor, *Mater. Today Commun.*, 2022, **31**, 103802, DOI: 10.1016/j.mtcomm.2022.103802.

32 K. R. Bhagya, K. R. Jyothi, V. N. Hegde, B. D. Prasad, H. Nagabhushana, S. C. Sharma and N. M. Nagabhushana, Orange-red emitting praseodymium doped yttrium-molybdate nanophosphors for multifunctional applications, *J. Sci.: Adv. Mater. Devices*, 2021, **6**, 234–244, DOI: 10.1016/j.jsamd.2021.02.002.

33 V. Vidyadharan, K. P. Mani, M. S. Sajna, C. Joseph, N. V. Unnikrishnan and P. R. Biju, Synthesis and luminescence characterization of Pr^{3+} doped $Sr_{1.5}Ca_{0.5}SiO_4$ phosphor, *Spectrochim. Acta, Part A*, 2014, **133**, 762–772, DOI: **10.1016/j.saa.2014.06.016**.

34 X. Tian, J. Li, H. Sheng, T. Li, L. Guo, C. Ji, Z. Huang, J. Wen, X. Liu, C. Li, J. Li and Y. Peng, Luminescence and optical thermometry based on silico-carnotite $Ca_3Y_2Si_3O_{12}$: Pr^{3+} phosphor, *Ceram. Int.*, 2022, **48**, 3860–3868, DOI: **10.1016/j.ceramint.2021.10.171**.

35 Y. Hu, F. Zhou, X. Tian, C. Ji, Z. Huang, J. Wne, F. Luo, Z. Chen, X. Liu and Y. Peng, $CaSnO_3$: Pr^{3+} phosphor for new application in temperature sensing, *Spectrochim. Acta, Part A*, 2020, **243**, 118799, DOI: **10.1016/j.saa.2020.118799**.

36 B. C. Jamalaiah, N. Madhu, A. S. N. Reddy, P. Gawas and V. Nutalapati, Structural and optical analysis of $YAl_3(BO_3)_4$: Pr^{3+} phosphors for lighting applications, *Optik*, 2022, **268**, 169744, DOI: **10.1016/j.ijleo.2022.169744**.

37 X. Wu, L. Du, Q. Ren and O. Hai, Enhancing the blue luminescence behaviour of the Na^+ co-doped novel $LiLaSiO_4$: ξTm^{3+} phosphor, *Polyhedron*, 2021, **202**, 115209, DOI: **10.1016/j.poly.2021.115209**.

38 A. P. de Azevedo Marques, R. Künzel, N. K. Umisedo, R. M. Latini, E. M. Yoshimura and E. Okuno, Tm^{3+} doped barium molybdate: A potential long-lasting blue phosphor, *J. Alloys Compd.*, 2018, **735**, 707–717, DOI: **10.1016/j.jallcom.2017.10.225**.

39 J. Pisarska, W. A. Pisarski, D. Dorosz and J. Dorosz, Spectroscopic properties of Pr^{3+} and Er^{3+} ions in lead-free borate glasses modified by BaF_2, *Opt. Mater.*, 2015, **47**, 548–554, DOI: **10.1016/j.optmat.2015.06.037**.

40 J. Pisarska, W. A. Pisarski, D. Dorosz and J. Dorosz, Spectral analysis of Pr^{3+} doped germanate glasses modified by BaO and BaF_2, *J. Lumin.*, 2016, **171**, 138–142, DOI: **10.1016/j.jlumin.2015.11.023**.

41 Kenry, Y. Duan and B. Liu, Recent advances of optical imaging in the second near-infrared window, *Adv. Mater.*, 2018, **30**, 1802394, DOI: **10.1002/adma.201802394**.

42 J. Zhao, D. Zhong and S. Zhou, NIR-I-to-NIR-II fluorescent nanomaterials for biomedical imaging and cancer therapy, *J. Mater. Chem. B*, 2018, **6**, 349–365, DOI: **10.1039/C7TB02573D**.

43 Y. Fan and F. Zhang, A new generation of NIR-II probes: Lanthanide-based nanocrystals for bioimaging and biosensing, *Adv. Opt. Mater.*, 2019, **7**, 1801417, DOI: **10.1002/adom.201801417**.

44 Z. Qu, J. Shen, Q. Li, F. Xu, F. Wang, X. Zhang and C. Fan, Near-IR emissive rare-earth nanoparticles for guided surgery, *Theranostics*, 2020, **10**, 2631–2644, DOI: **10.7150/thno.40808**.

45 C. Ma, H. Liu, F. Ren, Z. Liu, Q. Sun, C. Zhao and Z. Li, The second near-infrared window persistent luminescence for anti-counterfeiting application, *Cryst. Growth Des.*, 2020, **20**, 1859–1867, DOI: **10.1021/acs.cgd.9b01575**.

46 C. Li, G. Chen, Y. Zhang, F. Wu and Q. Wang, Advanced fluorescence imaging technology in the near-infrared-II window for biomedical applications, *J. Am. Chem. Soc.*, 2020, **142**, 14789–14804, DOI: **10.1021/jacs.0c07022**.

47 Y. Zhang, S. Zhang, Z. Zhang, L. JI, J. Zhang, Q. Wang, T. Guo, S. Ni, R. Cai, X. Mu, W. Long and H. Wang, Recent progress on NIR-II photothermal therapy, *Front. Chem.*, 2021, **9**, 728066, DOI: **10.3389/fchem.2021.728066**.

48 Y. Yang, D. Tu, Y. Zhang, P. Zhang and X. Chen, Recent advances in design of lanthanide-containing NIR-II luminescent nanoprobes, *iScience*, 2021, **24**, 102062, DOI: **10.1016/j.isci.2021.102062**.

49 L. R. R. Nunes, H. P. Labaki, F. J. Caixeta and R. R. Gonçalves, Yb^{3+} influence on NIR emission from Pr^{3+}-doped spherical yttria nanoparticles for advances in NIR I and NIR II biological windows, *J. Lumin.*, 2022, **241**, 118485, DOI: **10.1016/j.jlumin.2021.118485**.

50 Y. Liu, W. Luo, R. Li, H. Zhu and X. Chen, Near-infrared luminescence of Nd^{3+} and Tm^{3+} ions doped ZnO nanocrystals, *Opt. Express*, 2009, **17**, 9748–9753, DOI: **10.1364/OE.17.009748**.

51 P. R. Diamente, M. Raudsepp and F. C. J. M. van Veggel, Dispersible Tm^{3+}-doped nanoparticles that exhibit strong 1.47 μm photoluminescence, *Adv. Funct. Mater.*, 2007, **17**, 363–368, DOI: **10.1002/adfm.200600142**.

52 J. Pisarska, M. Kowal, M. Kochanowicz, J. Żmojda, J. Dorosz, D. Dorosz and W. A. Pisarski, Influence of BaF_2 and activator concentration on broadband near-infrared luminescence of Pr^{3+} ions in gallo-germanate glasses, *Opt. Express*, 2016, **24**, 2427–2435, DOI: **10.1364/OE.24.002427**.